RESEARCH ON A REAL-TIME HYPERSPECTRAL ANOMALY DETECTION METHOD BASED ON CHESSBOARD TOPOLOGY

Qianqian Sun[1] , *Meiping Song*[2,1,*] , *Xudong Sun*[1] , *Yisha Liu*[1]

[1] Information and Technology College, Dalian Maritime University, Dalian 116026, China
[2] School of Innovation Design, Guangzhou Academy of Fine Arts, Guangzhou 510006, China

ABSTRACT

Hyperspectral anomaly detection identifies targets by exploiting subtle spectral differences between objects and their surroundings. As a mathematical framework for analyzing data structures, topology can capture the intrinsic characteristics of data without relying on distance metrics or statistical assumptions. Building on chessboard topology [1], this paper proposes the Real-Time Chessboard Topology-Based Hyperspectral Anomaly Detection (RTCTAD) algorithm. To enable continuous real-time processing, the proposed method introduces dynamic chessboard topology construction together with a sliding-window update strategy. Dynamic min-max tracking, segmented quantization, and density statistics are used to characterize the spectral distribution of the local background, while a dynamic background update mechanism allows the algorithm to adapt quickly to changing scenes. Experimental results on hyperspectral datasets demonstrate that RTCTAD outperforms existing real-time methods in both detection accuracy and processing efficiency.

Index Terms— Hyperspectral images; topology; real-time anomaly detection; chessboard topology

1. INTRODUCTION

Hyperspectral images (HSIs) jointly represent spatial and spectral information by capturing the reflectance of objects over contiguous spectral bands, making them widely applicable in military reconnaissance, environmental monitoring, mineral exploration, and crop disease detection. Hyperspectral anomaly detection (HAD) aims to identify anomalous targets without prior target information by exploiting spectral differences between anomalies and the surrounding background, and has become an important research topic in hyperspectral image interpretation.

Traditional hyperspectral anomaly detection methods generally rely on statistical assumptions or signal models. Statistical model-based methods characterize the background distribution to separate anomalies. The classical Reed-Xiaoli (RX) detector computes the Mahalanobis distance under a multivariate Gaussian assumption [2]. Representative extensions include Weighted RX (WRX) [3], which improves robustness through adaptive weighting, multi-window modeling, and iterative anomaly suppression, and Kernel RX (KRX) [4], which enhances anomaly separability via kernel mapping, while cluster-assisted KRX further reduces computational cost [5].

Representation-based HAD methods identify anomalies according to the reconstruction residual of a background dictionary, with sparse representation (SR) and collaborative representation (CR) being the two main paradigms. The Collaborative Representation Detector (CRD) [6] constructs a dual-window background dictionary and improves target modeling through collaborative representation, while Low-Rank and Sparse Matrix Decomposition (LRaSMD) decomposes hyperspectral data into low-rank background, sparse anomaly, and noise components.

In recent years, deep learning has shown great potential for hyperspectral target detection. Representative methods include the meta-learning Siamese network (MLSN) [7], which improves model adaptability, HTD-Net [8], which alleviates the dependence on large-scale training samples, and a dual-stream convolutional network [9], which combines hybrid sparse representation with prior target spectra for target detection. In addition, Background Learning with Target Suppression Constraint (BLTSC) [10] performs unsupervised target detection by reconstructing the background with an adversarial autoencoder, while Spectral Contrastive Learning for Hyperspectral Target Detection (SCLHTD) [11], [12] exploits spectral augmentation and contrastive learning to learn discriminative spectral representations.

To meet the demand for lightweight real-time hyperspectral anomaly detection, various real-time HAD methods have been developed. Zhao et al. introduced recursive RX-based detectors (RTC-R-RXD and RTC-K-RXD) by combining Kalman filtering with the Woodbury lemma [13], and further proposed RTKRXD using a recursive polynomial kernel for nonlinear background – target separation [14]. Subsequent studies developed local real-time detectors based on sliding-window covariance estimation [15], Cholesky decomposition-based kernel detection [16], and finite Markov modeling [17]. Liu et al. further proposed RTMLMB-RAD, which reduces computational complexity through recursive block matrix inversion for lightweight spectral imaging applications [18]. These studies indicate that exploiting the sequential characteristics of hyperspectral

data is an effective strategy for reducing computational cost and improving processing efficiency.

This paper proposes a Real-Time Chessboard Topology-Based Hyperspectral Anomaly Detection (RTCTAD) algorithm by combining chessboard topology with a sliding-window-based update strategy. The proposed method enables online topological modeling of hyperspectral data streams without background distribution assumptions.

2. METHOD

2.1. Real-Time Chessboard Topology Construction

To enable pixel-wise real-time hyperspectral anomaly detection, the incoming spectral feature streams must be dynamically quantized online. At any time step *t*, let the newly arrived pixel vector be $x_t \in R^B$, t = 1,2…, where *B* is the number of spectral bands. For the *j*-th band (j = 1,2,...,B), the dynamic range bounds $[m_j^{min}(t),\ m_j^{max}(t)]$ are updated recursively via:

$$m_j^{max}(t) = max(m_j^{max}(t-1),\ x_t(j)) \quad (1)$$

$$m_j^{min}(t) = min(m_j^{min}(t-1),\ x_t(j)) \quad (2)$$

Based on the updated bounds, the dynamic range of the *j*-th band is evenly partitioned into *T* quantization levels (corresponding to the predefined number of rows in the topological chessboard structure), with a step size of $\Delta_j = \frac{m_j^{max}(t) - m_j^{min}(t)}{T-1}$. The quantization level index $l_j(t)$ for the incoming pixel in the *j*-th band is computed as:

$$l_j(t) = min(\left\lceil \frac{x_t(j) - m_j^{min}(t)}{\Delta_j} \right\rceil + 1,\ T) \quad (3)$$

To capture the dynamic evolution of local backgrounds while maintaining bounded computational complexity, a sliding window of size W_{size} is introduced to store the recent historical sample sequence. We define the chessboard topology counting matrix $C \in R^{T \times B}$, where each entry $C_{l,j}$ records the occurrence frequency of historical pixels within the current window falling into the *l*-th quantization level of the *j*-th band.

When a new pixel x_t arrives and the oldest pixel x_{old} is evicted from the window, matrix *C* adopts a dual-strategy efficient update mechanism: if the incoming pixel does not trigger an expansion of the global bounds [$m_j^{min}(t)$, $m_j^{max}(t)$], the topology update is achieved in O(1) complexity by simply decrementing the count at the quantization level of x_{old} by 1 and incrementing the count for x_t by 1; conversely, if the global bounds expand, all historical pixels in the current sliding window are re-quantized using the updated step size Δ_j , thereby accomplishing an adaptive reconstruction of the chessboard topological structure.

2.2. Real-Time Computation of BDV and CDV

For the quantized feature vector $l = [l_1, l_2, \ldots, l_B]$, to jointly extract frequency distribution and energy count information from the local chessboard topology, we construct the Basic Distribution Vector (BDV_d) and the Cumulative Distribution Vector (CDV_d). BDV describes the distribution of spectral components of the test pixel across different quantization levels, whereas CDV further incorporates background - count information for corresponding levels. Complementing the basic sparsity metric from the perspectives of level - distribution structure and background statistical characteristics, the two descriptors supply additional distribution information for anomaly scoring.

$$BDV_d(l) = \sum_{j=1}^{B} \delta(l_j - l) \quad (4)$$

$$CDV_d(l) = \sum_{j=1}^{B} C_{l_j j} \delta(l_j - l) \quad (5)$$

where l_j represents the quantization level of the *j*-th spectral band, and $\delta(x) = \begin{cases} 1, x = 0 \\ 0, x \neq 0 \end{cases}$.

The statistics of every w_r consecutive quantization levels are aggregated to construct $BDV(r)$ and $CDV(r)$, where *r* denotes the aggregated row index and *l* denotes the quantization level index. This operation effectively reduces the feature dimensionality while enhancing the robustness of the resulting descriptors.

$$BDV(r) = \sum_{k=(r-1)\cdot w_r+1}^{r\cdot w_r} BDV_d(l) \quad (6)$$

$$CDV(r) = \sum_{k=(r-1)\cdot w_r+1}^{r\cdot w_r} CDV_d(l) \quad (7)$$

In the weight computation module, the L_2 norms of the distribution frequency descriptor $BDV(r)$ and the cumulative count descriptor $CDV(r)$ for the *r*-th group are used to measure their descriptor energies, from which the band weight w_1 and the count weight w_2 are derived, respectively.

$$w_1 = \|BDV(r)\|_2, w_2 = \|CDV(r)\|_2 \quad (8)$$

2.3. Anomaly Score Computation and Anomaly Detection

The anomaly score fusion module combines the maximum count ratio, band distribution features, and count features to formulate the composite detection metric defined in (9). This metric enhances the discriminability between anomalies and the background, while the additive fusion strategy mitigates the influence of noise by avoiding overly restrictive constraints.

$$score = \left(\sum_{j=1}^{B} \frac{M_j}{C_{l_j(t),j} + \epsilon}\right) + w_1 + w_2 \quad (9)$$

where M_j denotes the maximum count of the j-th spectral band, $C_{l_j(t),j}$ represents the count corresponding to the quantization level of the current pixel in the j-th spectral band at time step t, w_1 and w_2 denote the band weight and the count weight, respectively, and ϵ is a numerical stability constant introduced to prevent division-by-zero errors.

The anomaly score is generated immediately upon the arrival of each pixel, enabling pixel-wise real-time anomaly detection.

3. EXPERIMENTAL DESIGN

This section evaluates the effectiveness and superiority of the proposed RTCTAD algorithm through comprehensive comparative experiments. The evaluation focuses on two aspects: detection performance and computational efficiency. The proposed method is compared with both conventional batch-processing anomaly detection methods and existing real-time anomaly detection algorithms. All experiments were conducted using MATLAB R2022b on a workstation equipped with an Intel Core i7-12700K CPU and 32 GB of RAM.

3.1. Experimental Results and Analysis

This section presents the experimental results and analyzes the detection performance of the proposed RTCTAD.

3.1.1. Comparison of Detection Maps

Fig. 1 shows the anomaly detection results of different methods on the San Diego dataset, where small aircraft are embedded in highly structured backgrounds, including runways, roads, and building rooftops, making anomaly detection particularly challenging.

RX detects most aircraft but with weak anomaly responses and low target-to-background contrast. LRX and LRASR generate strong responses over structured background regions, resulting in numerous false alarms. CRD suffers from blurred target boundaries, while CNN detects most targets but still produces noticeable background false alarms. Compared with these methods, CTAD highlights the anomalous targets more effectively while suppressing background responses.

Among the real-time methods, FMLRT-RAD produces low-saliency anomaly responses, RTK-RAD achieves good background suppression but weak anomaly responses, and CRXD provides limited target-to-background contrast. In contrast, the proposed RTCTAD generates more prominent and spatially consistent anomaly responses, with only a few strip-shaped false alarms along highly structured boundaries caused by abrupt spectral variations during streaming processing.This phenomenon mainly stems from the inherent limitation of the real - time streaming processing mechanism: it can only rely on historical information and cannot foresee future pixels. Therefore, when the scan line crosses the boundary between two distinctly different ground objects, such sharp jumps in material spectra will be judged by the model as "sudden anomalies" that disrupt the stable distribution of the current background, thereby triggering high responses instantaneously within the boundary transition zone.

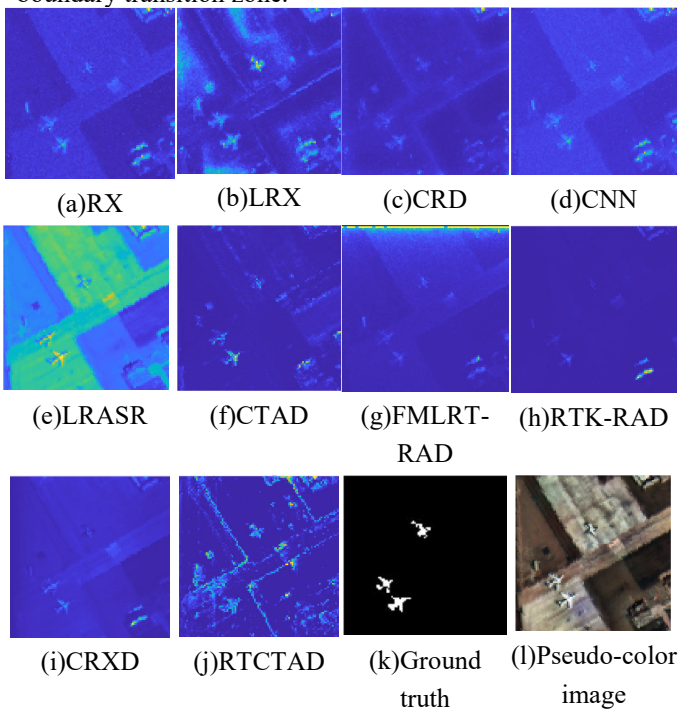


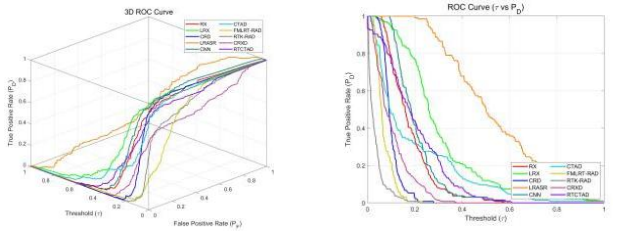
Fig. 1. Detection Results on the San Diego Dataset

3.1.2. Comparison of 3D-ROC Curves, AUC Metrics, and Computational Time

Fig. 2 compares the 3D-ROC and 2D-ROC curves of the evaluated methods on the San Diego dataset. Table I summarizes the AUC metrics and computational time of the nine hyperspectral anomaly detection algorithms, including five offline methods and four real-time methods. The best and second-best results within each category are highlighted in bold and underlined, respectively.

Overall, compared with the other real-time methods, the proposed RTCTAD consistently achieves the best or second-best performance on the San Diego dataset in terms of the AUC metrics. Moreover, it remains competitive with several offline methods on multiple evaluation metrics. As shown in Fig. 2, the ROC curves of RTCTAD closely

approach those of the conventional offline detectors, while the quantitative results in Table I further demonstrate its strong anomaly enhancement capability and overall detection performance.



(a)3D-ROC (b)2D-ROC Curve (P_D vs. τ)

(c)2D-ROC Curve (P_D vs. P_F) (d)2D-ROC Curve (P_F vs. τ)

Fig. 2. 3D-ROC and 2D-ROC Curves on the San Diego Dataset

Table I. AUC Values and Running Time on the San Diego Dataset

	Detector	AUC(P_D, P_F)	AUC(P_D, τ)	AUC(P_F, τ)	AUC(TD)	AUC(BS)	AUC(SNPR)	AUC(TDBS)	AUC(ODP)	Running time(s)
	RX	0.9403	0.1778	0.0589	1.1181	0.8814	3.0176	0.1189	1.0592	0.032
	LRX	0.9287	0.3054	0.0762	**1.2341**	0.8525	4.0082	**0.2292**	**1.1579**	5.889
Offline	CRD	0.8172	0.3475	0.2582	1.1647	0.5590	1.3459	0.0893	0.9065	8.081
methods	LRASR	0.6972	**0.5294**	0.3837	1.2266	0.3136	1.3798	0.1457	0.8429	5.062
	CNN	0.9505	0.2021	0.0885	1.1527	0.8620	2.2837	0.1136	1.0642	0.904
	CTAD	**0.9563**	0.1886	**0.0198**	1.1448	**0.9365**	**9.5235**	0.1688	1.1250	0.475
	FMLRT-RAD	0.7815	0.0692	0.0565	0.8507	0.7249	1.2239	0.0127	0.7941	0.630
Real-time	RTK-RAD	0.8920	0.0319	**0.0062**	0.9239	**0.8858**	5.1239	0.0257	0.9177	0.083
methods	CRXD	0.7731	0.1020	0.0411	0.8751	0.7321	2.4845	0.0609	0.8341	9.206
	RTCTAD	**0.9072**	**0.1970**	0.0323	**1.1042**	0.8749	**6.1060**	**0.1647**	**1.0719**	0.150

In addition, the running time comparison reveals significant differences in computational efficiency. Representation learning and reconstruction-based methods (CRD, CRXD, and LRASR) require the longest running time due to pixel-wise optimization or sparse/low-rank decomposition, while LRX is also computationally expensive because of its sliding-window-based local modeling. In contrast, the CNN-based method achieves efficient inference, and CTAD, FMLRT-RAD, and RTK-RAD provide a better balance between detection accuracy and computational efficiency.

RX consistently achieves the shortest running time because it only computes the global mean, covariance matrix, and Mahalanobis distance, which can be efficiently implemented through optimized matrix operations. However, its reliance on global statistical modeling limits its applicability to streaming data and complex backgrounds.

The proposed RTCTAD requires only 0.150 s to process the entire dataset, significantly outperforming the original CTAD and approaching the efficiency of RTK-RAD.

Computational Complexity Analysis: Let $P = M \times N$ denote the total number of pixels, B the number of spectral bands, and W the number of pixels in a local window. Based on the implementations used in this study, RX and LRX require $O(PB^2 + B^3)$ and $O(PWB^2 + B^3)$, respectively, due to global and local covariance estimation. CRD performs a local reconstruction for each pixel and has a complexity of $O(P(BS^2 + S^3))$, where S is the local dictionary size, while LRASR involves iterative low-rank and sparse decomposition with complexity dependent on the dictionary size and iteration number. The implemented FMLRT-RAD, RTK-RAD, and CRXD require repeated matrix operations, with complexities of approximately $O(PB^2 + MB^3)$, $O(T_{init}B^3 + PB^2)$, and $O(PB^3)$, respectively. CTAD performs batch processing over the entire image. In contrast, RTCTAD requires only $O(B)$ operations for a normal incoming pixel, yielding $O(PB)$ overall complexity. When dynamic spectral bounds expand, re-quantization of the W_s historical samples introduces an additional $O(EW_sB)$ cost, where E is the number of boundary expansions. Thus, with fixed spectral dimensionality and window size, RTCTAD maintains approximately linear complexity with respect to the number of input pixels while supporting pixel-wise real-time processing.

4. CONCLUSION

This paper presents a real-time chessboard topology-based anomaly detection algorithm for hyperspectral images. The proposed method processes pixel sequences using a sliding-window mechanism and maintains dynamically updated data structures to track changes in pixel hierarchy, enabling real-time processing of continuously acquired hyperspectral data. A chessboard data structure is employed to characterize the distribution of pixel hierarchies, while the maximum and minimum vectors are used to determine hierarchical levels, preserving local structural information and adapting to dynamic data variations. Furthermore, the BDV and CDV descriptors compress high-dimensional spectral features into compact and representative low-dimensional features. Feature weighting is incorporated to balance the contributions of different descriptors, allowing the anomaly score to more accurately reflect the degree of abnormality.

Experimental results on the representative San Diego hyperspectral dataset demonstrate that the proposed method achieves high detection accuracy while substantially improving computational efficiency compared with the

original batch-processing CTAD algorithm. Moreover, compared with existing real-time anomaly detection methods, RTCTAD exhibits superior detection performance and robustness. The comprehensive evaluation based on 3D-ROC metrics further verifies its advantages in threshold robustness, background suppression, and practical applicability.

Future work will focus on further improving detection accuracy and enhancing background suppression in complex structural regions, thereby enabling more robust and reliable anomaly detection across diverse hyperspectral imaging scenarios.

5. REFERENCES

[1] L. Gao, X. Sun, X. Sun, L. Zhuang, Q. Du, and B. Zhang, "Hyperspectral anomaly detection based on chessboard topology," IEEE Trans. Geosci. Remote Sens., vol. 61, Art. no. 5505016, 2023.

[2] I. S. Reed and X. Yu, "Adaptive multiple-band CFAR detection of an optical pattern with unknown spectral distribution," *IEEE Trans. Acoust., Speech, Signal Process*., vol. 38, no. 10, pp. 1760-1770, Oct. 1990.

[3] Q. Guo, B. Zhang, Q. Ran, et al., "Weighted-RXD and linear filter-based RXD: Improving background statistics estimation for anomaly detection in hyperspectral imagery," *IEEE J. Sel. Top. Appl. Earth Observ. Remote Sens*., vol. 7, no. 6, pp. 2351-2366, Jun. 2014.

[4] H. Kwon and N. M. Nasrabadi, "Kernel RX-algorithm: A nonlinear anomaly detector for hyperspectral imagery," *IEEE Trans. Geosci. Remote Sens*., vol. 43, no. 2, pp. 388-397, Feb. 2005.

[5] J. Zhou, C. Kwan, B. Ayhan, et al., "A novel cluster kernel RX algorithm for anomaly and change detection using hyperspectral images," *IEEE Trans. Geosci. Remote Sens*., vol. 54, no. 11, pp. 6497-6504, Nov. 2016.

[6] W. Li and Q. Du, "Collaborative representation for hyperspectral anomaly detection," *IEEE Trans. Geosci. Remote Sens.*, vol. 53, no. 3, pp. 1463-1474, Mar. 2015.

[7] Y. Wang, X. Chen, F. Wang, M. Song, and C. Yu, "Meta-learning-based hyperspectral target detection using Siamese network," *IEEE Trans. Geosci. Remote Sens*., vol. 60, pp. 1-13, 2022.

[8] G. Zhang, S. Zhao, W. Li, Q. Du, Q. Ran, and R. Tao, "HTD-Net: A deep convolutional neural network for target detection in hyperspectral imagery," *Remote Sens.*, vol. 12, no. 9, Art. no. 1489, 2020, doi: 10.3390/rs12091489.

[9] D. Zhu, B. Du, and L. Zhang, "Two-stream convolutional networks for hyperspectral target detection," *IEEE Trans. Geosci. Remote Sens.*, vol. 59, no. 8, pp. 6907-6921, Aug. 2021.

[10] W. Xie, X. Zhang, Y. Li, K. Wang, and Q. Du, "Background learning based on target suppression constraint for hyperspectral target detection," *IEEE J. Sel. Top. Appl. Earth Observ. Remote Sens.*, vol. 13, pp. 5887-5897, 2020.

[11] X. Chen, Y. Wang, and Z. Che, "Contrastive learning for hyperspectral target detection," in *Proc. IEEE Int. Geosci. Remote Sens. Symp. (IGARSS)*, 2022, pp. 887-890.

[12] Y. Wang, X. Chen, E. Zhao, and M. Song, "Self-supervised spectral-level contrastive learning for hyperspectral target detection," *IEEE Trans. Geosci. Remote Sens*., vol. 61, pp. 1-16, 2023.

[13] X. Li, Y. Wang, and C. Zhao, "A novel real-time hyperspectral anomaly detection algorithm," *J. Infrared Millim. Waves*, vol. 34, no. 1, pp. 114-121, 2015, doi: 10.3724/SP.J.1010.2015.00114.

[14] C. Zhao, W. You, and B. Qi, "Real-time hyperspectral anomaly detection algorithm using polynomial recursive kernel," *Acta Opt. Sin*., vol. 36, no. 2, Art. no. 0228002, 2016, doi: 10.3788/AOS201636.0228002.

[15] L. Zhao, W. Lin, Y. Wang, et al., "Recursive local summation of RX detection for hyperspectral image using sliding windows," *Remote Sens*., vol. 10, no. 1, pp. 1-17, 2018.

[16] C. Zhao and X.-F. Yi, "Fast real-time kernel RX algorithm based on Cholesky decomposition," *IEEE Geosci. Remote Sens. Lett*., vol. 15, no. 11, pp. 1760-1764, Nov. 2018.

[17] S. Liu, M. Song, B. Xue, C.-I. Chang, and M. Zhang, "Hyperspectral real-time local anomaly detection based on finite Markov via line-by-line processing," *IEEE Trans. Geosci. Remote Sens*., vol. 62, Art. no. 5503520, pp. 1-20, 2024.

[18] S. Liu, "Research on real-time processing methods for hyperspectral anomaly detection," Ph.D. dissertation, Dept. of Information Science and Technology, Dalian Maritime Univ., Dalian, China, 2024.